JOURNAL OF AIRCRAFT
Vol. 32, No. 4, July–August 1995

Vortex Control over Sharp-Edged Slender Bodies

D. Gangulee* and T. Terry Ng†
University of Toledo, Toledo, Ohio 43606

An experimental study of controlling the flow over highly slender, sharp-edged bodies at high angles of attack was conducted. Four forebodies with similar planform shape will be studied: an 80-deg sweep delta wing, a diamond-shaped forebody, and two chine forebodies with different cross sections. A small flat plate used as a flow deflector on the leeward side was used as the vortex control device. Significant controlled forces and moments can be produced on all the forebodies, especially at high angles of attack. The optimal position of a deflector is inboard of the leading edge for the delta wing, and at the leading edge for the other forebodies. On the delta wing, the deflector induces a vortex that situates closer to the surface than the vortex on the side without the deflector. The opposite is true for the other forebodies. Changing the height, location, deflection angle, and shape of the deflector alter these vortex behaviors, which in-turn changes the forces and moments. At very high angles of attack the deflectors promote vortex breakdown, and the control effectiveness thereby is diminished.

Nomenclature

b = base wingspan
C_l = rolling moment coefficient, rolling moment/(qSb)
C_m = pitching moment coefficient, pitching moment about the trailing edge/(qSc)
C_N = normal force coefficient, normal force/(qS)
C_n = yawing moment coefficient, yawing moment about the model base/(qSc)
c = wing chord
h = flow deflector height
h^* = h/b
L = left side from the pilot's view
l = flow deflector length
l^* = l/c
q = freestream dynamic pressure
R = right side from the pilot's view
S = planform area
V_∞ = freestream velocity
x = chordwise position from the apex
x^* = x/c
α = nominal angle of attack
β = yaw angle, right positive
ϕ = surface ray angle from the model leeward centerline
ψ = deflector angle from the wing surface

I. Introduction

MODERN fighter aircraft are required to operate in a flight regime that requires the maximum maneuverability and controllability possible to be effective in the combat arena. Requirements for high maneuverability necessarily dictate that aircraft must fly at high angles of attack where the aerodynamics are dominated by separated and vortex flows. These vortex flows provide significant enhancement to the aerodynamic performance of the airframe. However, they can also cause significant problems in controllability. One of the major sources of aircraft control problems at high angles of attack is associated with the vortex pair produced by the typical slender aircraft forebody at medium-to-high angles of attack. Specifically, the interaction between the closely spaced vortices results in flow asymmetries such as asymmetric vortex liftoff and breakdown. The asymmetries in turn can induce strong rolling, pitching, and yawing moments that can lead to static and dynamic stability problems such as yaw departure, uncontrolled pitch-up and deep stall, and wing rock. If there are means to control locally these vortex-flows on the aircraft, one should be able to use this powerful force input to enhance overall airplane controllability.

Recent research efforts[1–9] on fighter-type aircraft indicated that some of the most promising methods for forebody vortex control are movable forebody strakes, rotatable nosetip devices, blowing/suction on the forebody surface, and different forms of small perturbations. Most of the research effort to-date on vortex control techniques has been focused on generic or specific fighter aircraft configurations representing present-day aircraft. Future aircraft configurations, however, are tending toward shapes and concepts that are beyond the present aerodynamic database. In particular, the desire for low observability dictates that the fuselage and forebody cross-sectional shape to be more chine-shaped, rather than circular or elliptic.

Some recent experimental studies on the flow over a chine forebody are discussed in Refs. 10–13. The purpose of these experiments was to understand the nature of the forebody vortices on a chine forebody and the interactions of the forebody vortices with the wing. The studies mainly focused on a particular generic forebody geometry. The effect of the forebody vortices on the overall flowfield, in particular their influence on the wing flow, is substantial. An aircraft configuration incorporating a chine forebody was found to possess both good static lateral and directional stability characteristics and low wing-rock amplitude. A potential pitch-up problem due to the strong forebody vortices was revealed.

Examples of recent studies on chine forebody vortex control are discussed in Refs. 14–16. Guyton et al.[14] studied the control of forebody vortices by blowing from a slot located along the leading edge. Large pressure asymmetry was found on the wing due to the interaction between the wing flow and the asymmetric breakdown of the forebody vortices. The results indicate that effective lateral control can potentially be provided by blowing at high angles of attack. Iwanski[15] studied the control of chine forebody vortex breakdown using spoiler-like devices located on the leeward surface. The method was found to be ineffective. Rao and Sharma[16] investigated using a deployable strake as a control device. The strake was located on the windward side and extended along the entire forebody length. The experiment was conducted on a diamond-shaped forebody. Various strake geometries were tested. The method

Received May 25, 1994; revision received Dec. 19, 1994; accepted for publication Dec. 27, 1994. Copyright © 1995 by the American Institute of Aeronautics and Astronautics, Inc. All rights reserved.

*Graduate Assistant, Department of Mechanical Engineering.
†Associate Professor, Department of Mechanical Engineering. Member AIAA.

was shown to be potentially effective in controlling both the normal and side forces.

The important elements of a forebody flow are the primary flow and separation, the reattachment flow and the secondary separation, and the primary and secondary vortices. These elements are not independent, and altering one will also alter the others. In addition, a control applied locally will lead to changes along the entire vortex. Hence, there is no doubt more than one means by which the vortex flow can be controlled. A sufficiently strong perturbation can of course alter the forebody flow under any circumstances. Thus, the main question on a control is perhaps the efficiency of the particular method. There may be certain fundamental principles that are common to various control concepts that make one method more effective for a particular forebody design. A better understanding of the basic fluid mechanisms of vortex control will lead to more efficient control strategies for different forebody designs.

One of the main differences between a smooth forebody and a chine forebody is that the primary separation on the latter is, for all practical purposes, fixed without a large leading-edge extension such as a flap. This precludes many conventional separation controls from being means of forebody vortex control. The control method investigated in the present study is a deployable flow deflector located on the leeward side. The specific technical objectives of the study are 1) to investigate some effects of slender body cross-sectional shape on vortex asymmetry and controllability and 2) to identify some means of controlling the vortex flows over sharp-edged slender bodies at high angles of attack.

This article will focus on the results of an 80-deg delta wing and a diamond cross section forebody, each tested separately. The 80-deg delta wing has been studied rather extensively. The basic characteristics are therefore well-known. The diamond forebody represents a generic chine geometry that has been investigated in some previous studies and is being considered as representative of a potential forebody geometry for future aircraft.

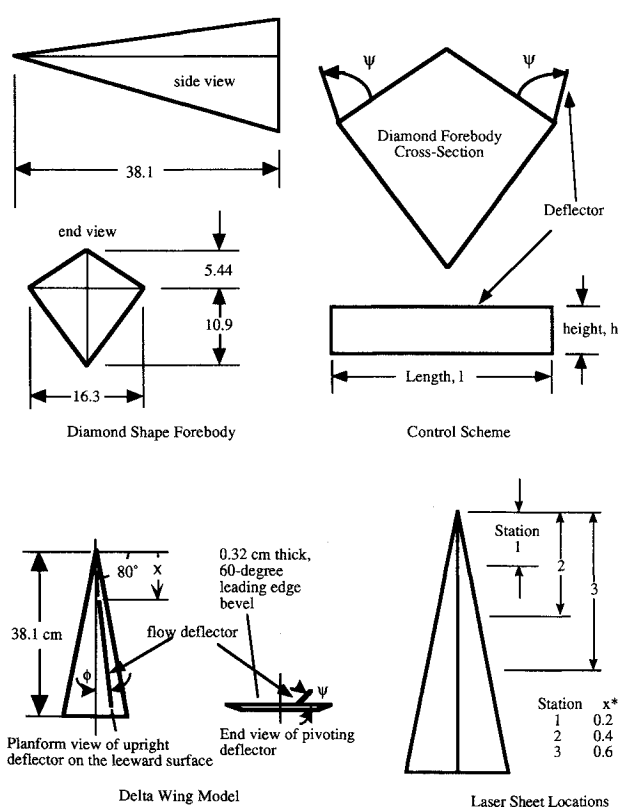

Fig. 1 Schematics of the models (dimensions in cm).

II. Approach

The experiment was performed in the University of Toledo 3 × 3-ft Subsonic Wind Tunnel. Tests were conducted at a tunnel dynamic pressure of 0.48 kPa, corresponding to a chord Reynolds number of 7.1×10^5. An 80-deg delta wing and a diamond forebody model were used and are shown schematically in Fig. 1 along with the control. Both models were 38.1 cm long. The delta wing model was constructed of 0.32-cm-thick aluminum plate with a 60-deg leading-edge bevel. The diamond forebody was constructed of galvanized metal sheets on an aluminum frame. The control scheme consisted of a thin rectangular plate placed along a ray from the leeward centerline of a model. The deflector parameters of interest are the length l, height h, deflection angle relative to the surface ψ, angular position relative to the leeward meridian ϕ, and the chordwise position x. Due to the large numbers of deflector parameters, the experiment was conducted by varying one parameter at a time.

Static force and moment measurements were carried out using a five-component (no axial force) strain-gauge moment balance. Smoke for off-surface flow visualizations is generated by a remote-controlled smoke generator located in the settling chamber upstream of the flow conditioners. In addition to the regular flood light illumination, a laser light sheet is used to provide cross-sectional views of the vortex flow. Flow visualization results are recorded using a 35-mm camera and a video camera. The images obtained are then digitized and analyzed.

III. Results and Discussions

A. Forces and Moments

1. *Effect of Ray Angle on the Controlled Moments*

The control moments of interest are the rolling moment for a delta wing and the yawing moment for a forebody. Figure 2 shows the effect of a deflector on the rolling moment on the delta wing. The deflector with $l^* = 0.54$ and $h^* = 0.047$ is placed at $x^* = 0.27$, $\psi = 90$ deg, and different ϕ (maximum $\phi = 10$ deg). In general, a deflector placed on the right side generates a negative (counterclockwise) rolling moment and vice versa. Thus, the deflector strengthens the vortex flow of the side it is on. The deflector becomes effective at $\alpha \approx 10$ deg, and peak values of C_l can be seen at $\alpha \approx 25$ and 40 deg. The effectiveness and behavior are relatively insensitive to the deflection ray angle position. Angles from 2 to 6 deg produce basically similar results, with a small reduction in effectiveness at $\phi = 8$ deg.

Figure 3 shows the effect of a deflector on the yawing moment of the diamond forebody. The deflector has dimensions of $l^* = 0.53$ and $h^* = 0.078$, and is placed at $x^* = 0.017$, $\psi = 90$ deg, and ϕ at 7-deg intervals (maximum $\phi = 21$ deg) from the leeward centerline. Unlike the delta wing where the

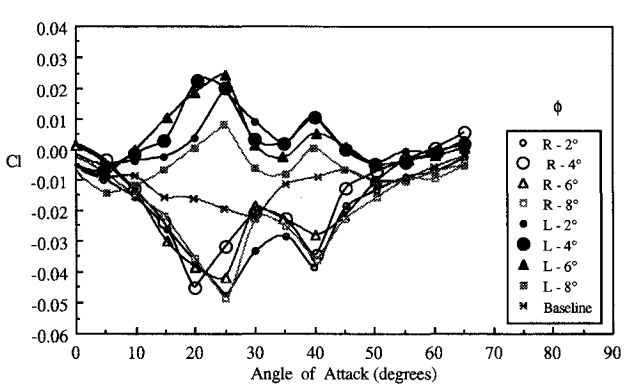

Fig. 2 Effect of deflector ray angle position on the rolling moment on the delta wing. Parameters: $l^* = 0.54$, $h^* = 0.047$, $x^* = 0.27$, $\psi = 90$ deg, and ϕ = variable.

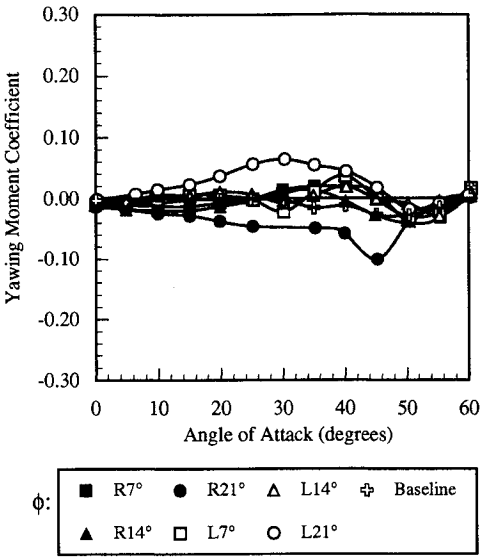

Fig. 3 Ray angle effect on the yawing moment on the diamond forebody. Parameters: $l^* = 0.53$, $h^* = 0.078$, $x^* = 0.017$, $\psi = 90$ deg, and ϕ = variable.

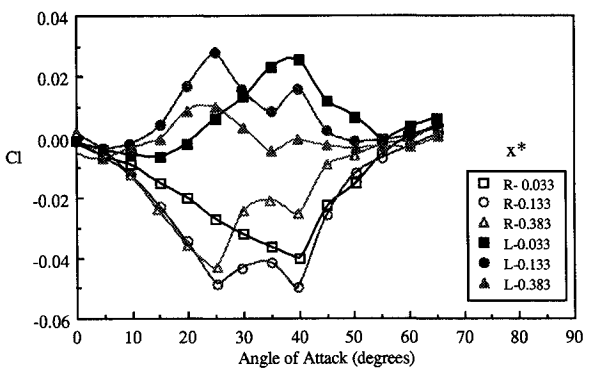

Fig. 4 Effect of deflector chordwise position on the rolling moment on the delta wing. Parameters: $l^* = 0.27$, $h^* = 0.071$, x^* = variable, $\psi = 90$ deg, and $\phi = 4$ deg.

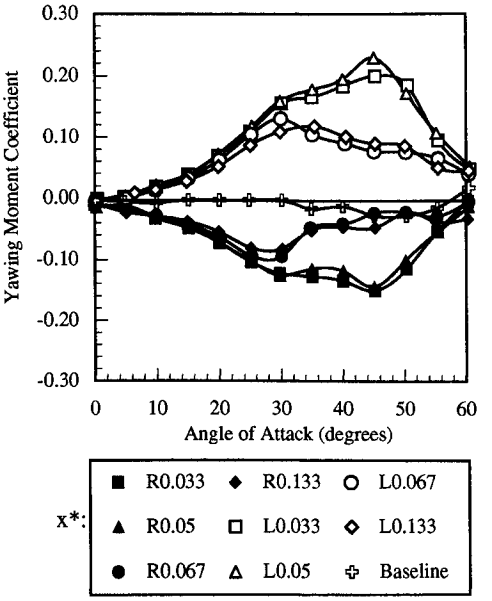

Fig. 5 Chordwise location effect on the yawing moment on the diamond forebody. Parameters: $l^* = 0.20$, $h^* = 0.078$, $\psi = 90$ deg, x^* = variable, and $\phi = 21$ deg.

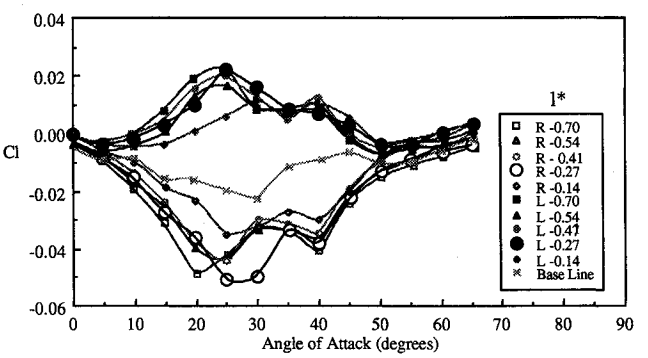

Fig. 6 Effect of deflector length on the rolling moment on the delta wing. Parameters: l^* = variable, $h^* = 0.071$, $x^* = 0.27$, $\psi = 90$ deg, and $\phi = 4$ deg.

most effective ray position is inboard of the leading edge, the most effective position is at the side edge of the diamond forebody. A deflector placed on the right side generates a negative yawing moment (to the left) and vice versa. Thus, in contrast to the delta wing, a deflector weakens the vortex of the side it is on. There is a noticeable left and right asymmetry in deflector effectiveness for angles of attack above 30 deg, which corresponds to the appearance of a baseline asymmetric yawing moment.

2. Effect of Chordwise Location

Figure 4 shows the effect of chordwise position on the delta wing for a deflector at $\phi = 4$ deg and $\psi = 90$ deg. Chordwise position x^* has a strong effect on C_l. Among the three locations tested, $x^* = 0.133$ is the most effective in providing control C_l over a wide range of α. Locating the deflector to a more backward position of $x^* = 0.383$ does not change the effectiveness at the lower α range, but the effectiveness at higher α are significantly reduced. Locating the deflecting to a more forward position of $x^* = 0.033$ has the opposite effect. The effectiveness at higher α are unaffected while that at lower α are reduced. Thus, for a given deflector geometry, there appears to be an optimum x^* location for control effectiveness.

Figure 5 shows the effect of the chordwise position on the diamond forebody for a deflector with $l^* = 0.20$, $h^* = 0.078$ at the model edge with $\psi = 90$ deg. Below $\alpha = 30$ deg the chordwise location has little effect on the control effectiveness. Above $\alpha = 30$ deg, however, there is a significant reduction in the effectiveness when x^* is increased from 0.05 to 0.067. Interestingly, the respective effectiveness does not change appreciably when x^* is increased to greater than 0.067 or reduced to less than 0.05. Again, for a given deflector geometry, there appears to be an optimum x^* location for control effectiveness.

3. Effect of Length

Figure 6 shows the effect of deflector length on the delta wing with a deflector at $\phi = 4$ deg, $\psi = 90$ deg, $x^* = 0.27$, and $h^* = 0.047$. A variation of l^* from 0.70 to 0.27 has little effects on the C_l generated. When l^* is reduced to 0.14, there is a noticeable reduction in the peak C_l near $\alpha = 20$ deg. At higher α, however, the effectiveness of the deflector is virtually the same as the other deflectors of greater lengths. Hence, the results indicate that the deflector can provide effective control even with relatively short lengths. This is especially true at high angles-of-attack range.

Figure 7 shows the effect of deflector length on the forebody with a deflector at the edge, $h^* = 0.078$, $\psi = 90$ deg, and $x^* = 0.033$. When the length was varied from l^* of 0.033 to 0.20 the effect of the deflector increases with deflector length, but the rate of increase is not linear and is relatively small for l^* from 0.13 to 0.20. Increasing l^* from 0.20 to 0.26 leads

to a reduction in the effectiveness at angles of attack above 30 deg. Hence, the results indicate that the deflector can provide effective control with relatively short lengths, and, there is an optimal length for a given deflector placement.

4. Effect of Height

The results indicate that the deflector can provide effective control even at a relatively short height. For instance, the h^* for the delta wing case shown in Fig. 4 can be changed from 0.047 to 0.095 without noticeably affecting the control effectiveness. Figure 8 shows the effect of deflector height on the diamond forebody with a deflector at the edge, $\psi = 90$ deg, $x^* = 0.133$, and $l^* = 0.26$. Above 25-deg angle of attack, the deflector loses its effectiveness when placed on the right side. Nevertheless, the magnitude of the yawing moment increases gradually with the deflector height over the entire angle-of-attack range. The highest height tested provides the highest control moment.

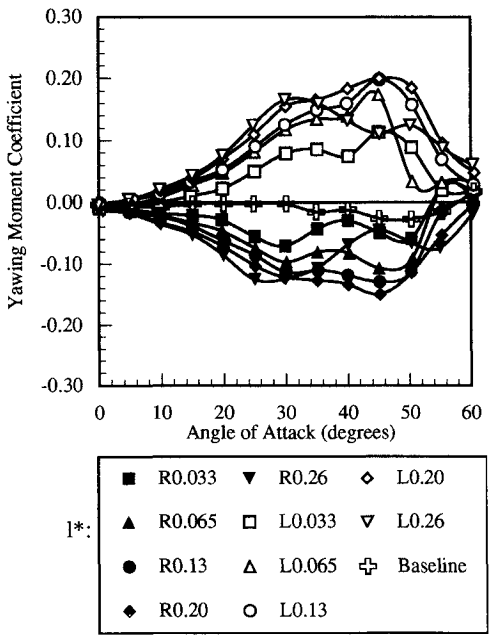

Fig. 7 Length effect on yawing moment on the diamond forebody. Parameters: l^* = variable, $h^* = 0.078$, $\psi = 90$ deg, $x^* = 0.033$, and $\phi = 21$ deg.

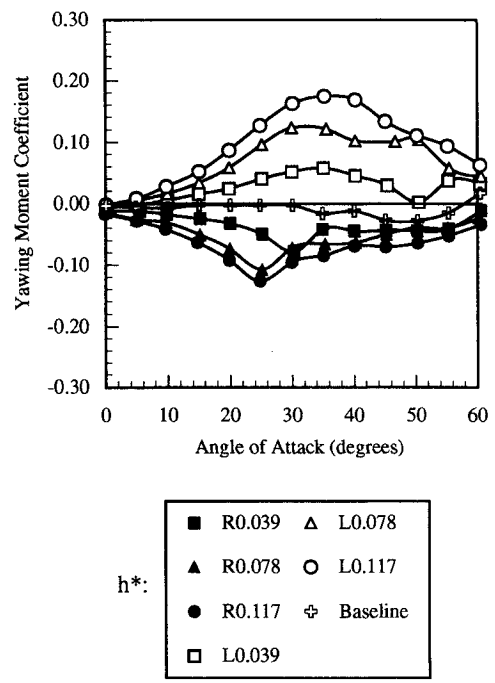

Fig. 8 Height effect on yawing moment on the diamond forebody. Parameters: $l^* = 0.26$, h^* = variable, $\psi = 90$ deg, $x^* = 0.133$, and $\phi = 21$ deg.

5. Effect of Deflector Angle

Figure 9 shows the effect of deflector angle ψ on the delta wing with a deflector at $\phi = 4$ deg and $x^* = 0.133$. A very gradual reduction in C_l can be seen when ψ is changed from 90 to 60 deg. This suggests that the height can be reduced and still provides the same maximum controlled moment. Below 60 deg, C_l reduces gradually with decreasing ψ. The result indicates a relatively well-behaved control characteristic between $\psi = 0$ to 60 deg, and, for this combination of deflector and model configurations, there is little reason to go beyond $\psi = 60$ deg. Similar results are obtained for the diamond forebody.

6. Effects on Other Moments

The effects of a deflector on the normal force and pitching moment on the delta wing and the forebody are relatively small. Changes from the baseline are noticeable only over the same angle range where the control is effective.

Figure 10 shows an example of the rolling moment of the diamond forebody. Below α of 35 deg, there is a positive

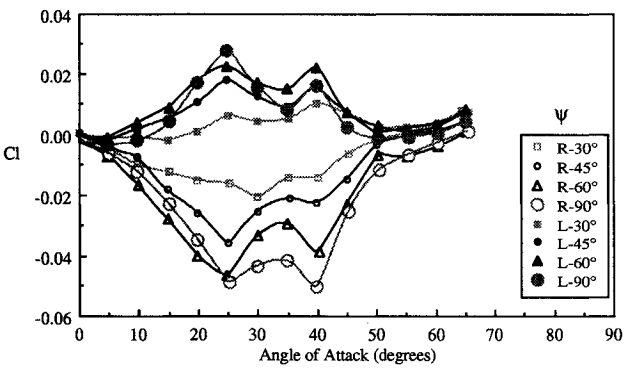

Fig. 9 Effect of deflector angle on the rolling moment on the delta wing. Parameters: $l^* = 0.27$, $h^* = 0.071$, $x^* = 0.133$, ψ = variable, and $\phi = 4$ deg.

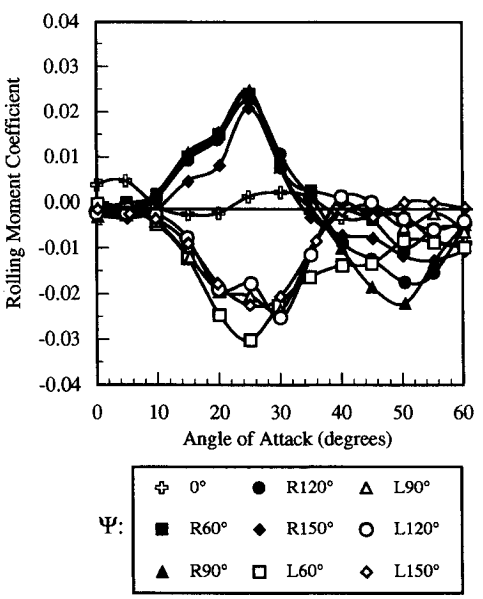

Fig. 10 Deflection angle effect on the rolling moment on the diamond forebody. Parameters: $l^* = 0.20$, h^* = tapered, $x^* = 0.05$, ψ = variable, and $\phi = 21$ deg.

coupling between the yawing and rolling moments. A positive yawing moment is associated with a positive rolling moment. Above $\alpha = 35$ deg, however, a negative coupling exists due to a reversal of the rolling moment.

B. Flow Visualizations

Figure 11 shows the vortex flows at three angles of attack for the delta wing model with a deflector at $\phi = 4$ deg on the right side. Only the left vortex is easily visible in the pictures due to the camera angle. At α of 30 and 40 deg, the deflector on the right causes the left vortex to lift farther from the wing surface compared with the baseline. Correspondingly, the right vortex moves closer to the surface. This asymmetry is expected to induce a negative rolling moment, which agrees with the C_l results presented earlier. The asymmetry is proportionally higher at the upstream location where the deflector is located than farther downstream. This leads to a curvature in the vortex trajectory that is visible at α below 40 deg. Note also that the maximum asymmetry exists where the rolling moment arm is relatively small. The magnitude of the rolling moment would therefore tend to understate the overall vortex asymmetry. At $\alpha = 50$ deg, vortex breakdown advances upstream over the wing, and the deflector has little visible effects on the vortices.

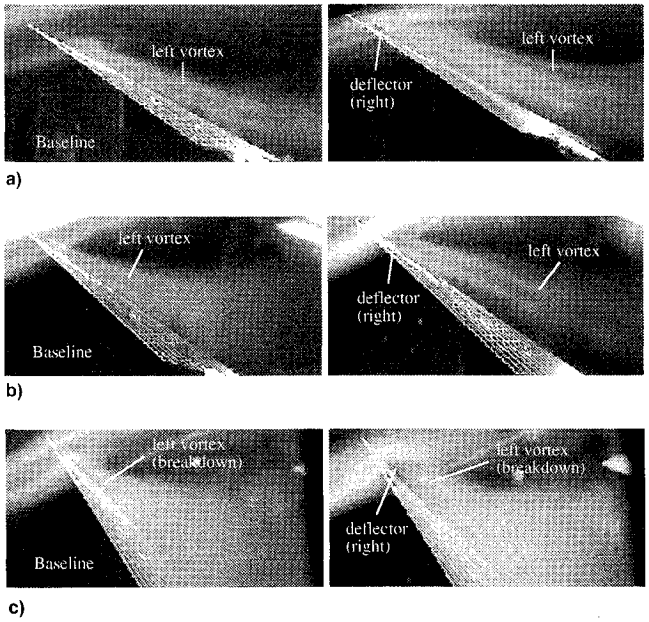

Fig. 11 Effect of a deflector on the vortex flow over the delta wing. Parameters: $l^* = 0.27$, $h^* = 0.071$, $x^* = 0.133$, $\psi = 90$ deg, and $\phi = 4$ deg. α = a) 30, b) 40, and c) 50 deg.

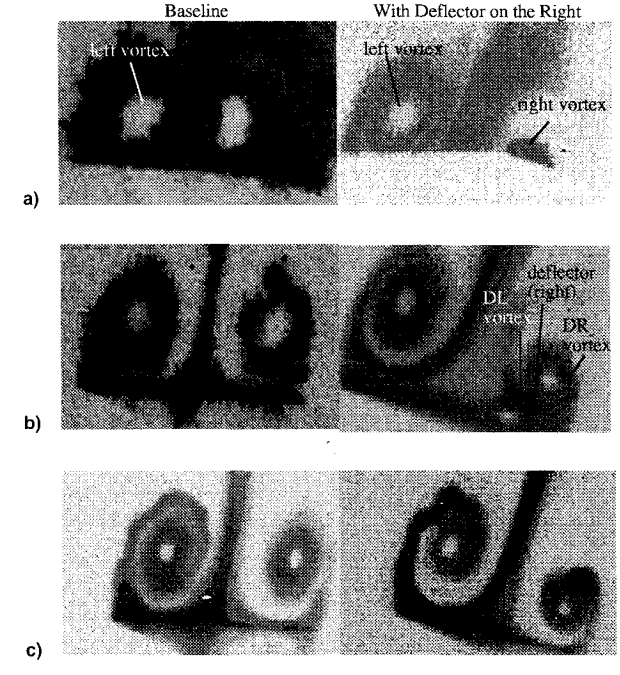

Fig. 12 Laser cross sections showing the effect of a deflector on the vortex flow over the delta wing at $\alpha = 20$ deg. Parameters: $l^* = 0.27$, $h^* = 0.071$, $x^* = 0.133$, $\psi = 90$ deg, and $\phi = 4$ deg. Stations a) 1, b) 2, and c) 3.

Figure 12 shows the laser cross sections at stations 1, 2, and 3 of the flow at the same deflector configuration as in Fig. 11. At $\alpha = 20$ deg, the deflector causes the formation of two vortices on the two sides of the deflector. These vortices on the left and right sides of the deflector are labeled as the DL and DR vortices respectively. The vortices have the same sense of rotation and merge to form one vortex at station 3. A position asymmetry between the left and right vortex can be seen at station 3. A similar effect of the deflector can be seen at other angles of attack. Above $\alpha = 30$ deg, the deflector promotes the breakdown of the vortex on the side with the deflector.

Figure 13 shows the vortex flows over the diamond forebody at angles of attack of 30, 40, and 50 deg. The model has a deflector located at the left leading edge, with $l^* = 0.20$, $h^* = 0.078$, $x^* = 0.033$, and $\psi = 90$ deg. The food light illuminated smoke flows show that a deflector on the left edge causes the left vortex to lift farther from the model surface compared with the baseline. Correspondingly, the right vortex moves closer to the surface. This asymmetry is expected to induce a positive yawing moment, which agrees with the C_n results. The asymmetry is proportionally higher at the upstream location near where the deflector is located than farther downstream. This leads to a visible curvature in the vor-

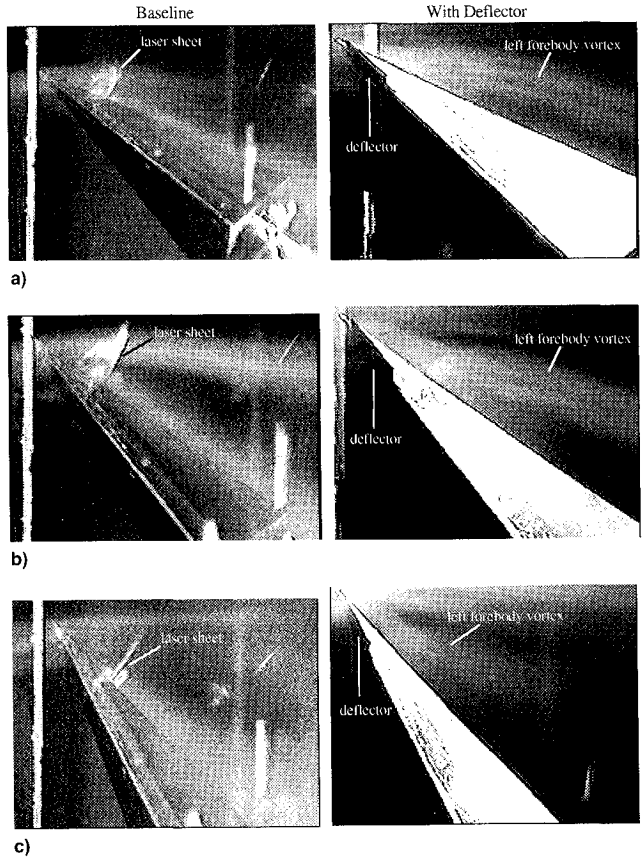

Fig. 13 Smoke visualization of the forebody vortex flows at different angles of attack. Parameters: $l^* = 0.20$, $h^* = 0.078$, $\psi = 90$ deg, $x^* = 0.033$, $\phi = 21$ deg. α = a) 30, b) 40, and c) 50 deg.

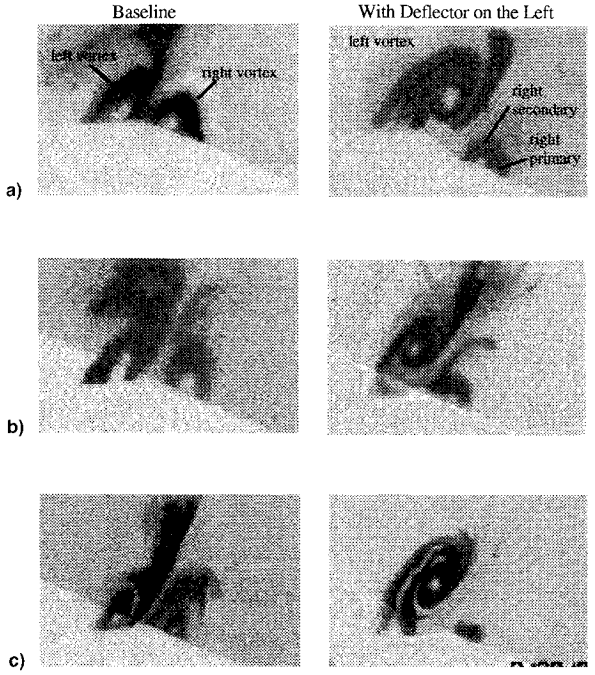

Fig. 14 Laser sheet visualization of the forebody vortex flows at 30-deg angle of attack. Parameters: $l^* = 0.20$, $h^* = 0.078$, $\psi = 90$ deg, $x^* = 0.033$, and $\phi = 21$ deg. Stations a) 1, b) 2, and c) 3.

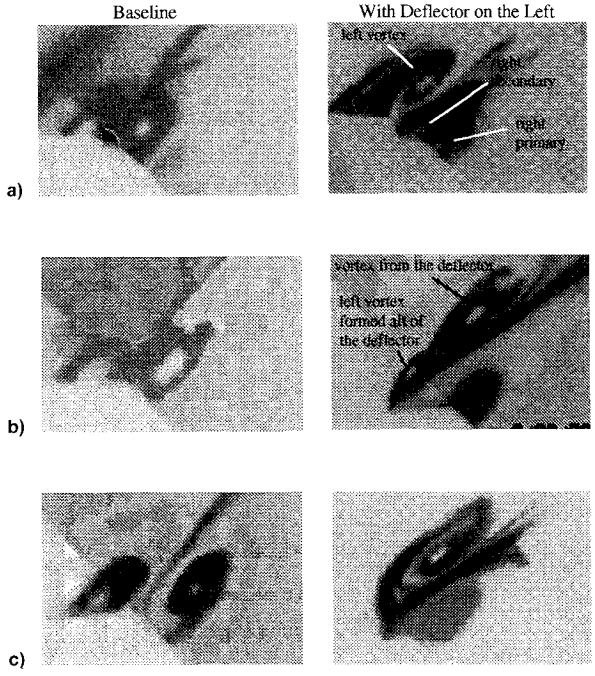

Fig. 15 Laser sheet visualization of the forebody vortex flows at 50-deg angle of attack. Parameters: $l^* = 0.20$, $h^* = 0.078$, $\psi = 90$ deg, $x^* = 0.033$, and $\phi = 21$ deg. Stations a) 1, b) 2, and c) 3.

tex trajectory. At $\alpha = 50$ deg, vortex breakdown occurs over the model and well upstream of the trailing edge.

The laser cross sections in Fig. 14 show the baseline flow and the flow with the deflector at $\alpha = 30$ deg. The left vortex is lifted from the surface due to the deflector on the left side. On the right side, the secondary flow separates along the top model edge to form a relatively strong secondary vortex situating alongside the right primary vortex. A large vortex asymmetry with the corresponding forces and moments are thereby induced.

At $\alpha = 40$ deg, the vortex flow behavior is similar to that at $\alpha = 30$ deg. Vortex breakdown occurs on the right side at

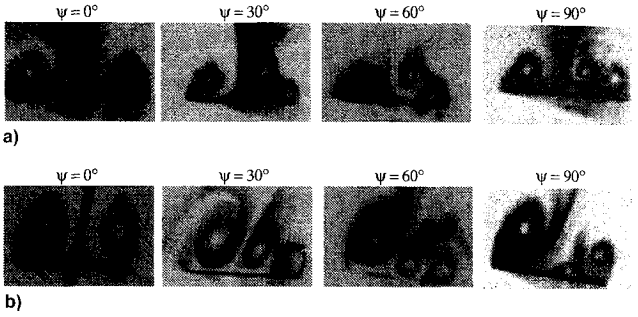

Fig. 16 Effect of deflector angle on the vortex flows over the delta wing at $\alpha = 10$ and 20 deg. Laser sheet located at station 2 just aft of the deflector. Parameters: $l^* = 0.27$, $h^* = 0.071$, $x^* = 0.133$, ψ = variable, $\phi = 4$ deg. α = a) 10 and b) 20 deg.

station 2. The vortex position asymmetry, however, remains significant at all three stations.

The laser cross sections in Fig. 15 show the baseline flow and the flow with the deflector at $\alpha = 50$ deg. The vortex flow behavior is again similar to that at $\alpha = 30$ deg. One can also see the formation of two distinct vortices on the side with the deflector. A vortex forms along the deflector. Downstream of the deflector another vortex forms along the leading edge of the forebody. The two vortices interact and eventually coalesce to form a single vortex, and the flow at station 3 becomes similar to that at $\alpha = 40$ deg.

Figure 16 shows the effect on the delta wing of deflector angle ψ for a deflector on the right side and at $\alpha = 10$ and 20 deg. At $\alpha = 10$ and 20 deg, changing ψ alters both the trajectory and strength of the DL vortex relative to the DR vortex, and thus, the overall flow asymmetry. At both α, $\psi = 60$ deg appears to produce DL and DR vortices that seem roughly similar in strength (based on the visually observed vortex sizes and spin rates) and relatively close to each other. This results in the deflector being most effective at $\psi = 60$ deg at $\alpha = 10$ and 20 deg. In addition to changing the vortex positions, the deflector promotes vortex breakdown on the side it is residing at high angles of attack. This combination of effects produces different controlled moments as shown in Fig. 10.

IV. Conclusions

An experimental study was performed to explore the potential of using flow deflectors to control the vortices over slender sharp-edged bodies at high angles of attack. The results are summarized below:

A. 80-Deg Delta Wing

The results on an 80-deg sweep wing indicate that well-behaved controlled moments can be produced using relatively small deflectors. The optimal position of a deflector is inboard of the leading edge. At moderate-to-high angles of attack, two vortices are trapped on both sides of the deflector. Past the trailing edge of the deflector the vortices coalesce to form a single vortex and a significant asymmetry in the forebody vortex flow is induced. At very high angles of attack, the deflector promotes the breakdown of the vortex on the side of the wing where it is located. Changing the height, location, and deflection angle of the deflector alter these vortex behaviors and in-turn changes the magnitude of forces and moments. Eventually, the advancement of breakdown diminishes the control effectiveness.

B. Diamond-Shaped Forebody

The results on a diamond forebody indicate that controlled moments can be produced by a small deflector placed on the leading edge. On the side with the deflector, the local flow is deflected and separates from the leading edge farther from

the leading edge than the case without the deflector. This creates a large local asymmetry between the two primary vortices. The asymmetric primary vortices in-turn induce an asymmetric secondary flow. On the side without the deflector where the primary vortex is close to the surface, the asymmetric leeward surface flow separates along the sharp top edge of the diamond forebody to form a strong secondary vortex. This strong local asymmetry eventually induces an asymmetry in the entire flowfield to produce the controlled forces and moments.

In contrast to the delta wing at high angles of attack, the deflector promotes the breakdown of the vortex on the opposite side of the diamond forebody. Thus, two forms of observable vortex asymmetry exist at this condition: 1) a position asymmetry that favors the side without the deflector, and 2) a breakdown asymmetry that favors the side with the deflector. These two asymmetries have counteracting effects on the controlled moments. Since the vortex breakdown occurs initially downstream (where the majority of the lateral moment is generated), it tends to affect the rolling moment sooner than the yawing moment. This accounts for the reversal in the coupling between the yawing and rolling moments at very high angles of attack.

C. Cross-Sectional Shape

A deflector has opposite effects on the delta wing and the diamond forebody. On the delta wing a deflector strengthens the vortex flow on the side it resides, while the opposite is true on the diamond forebody. One of the main differences between the delta wing and the diamond forebody is the sharp top edge on the latter. The flat leeward surface of a delta wing plays basically a neutral role in the secondary flow separation process. By placing a deflector inboard of the leading edge, two vortices with the same sense of rotation are trapped on the left and right sides of the deflector. This helps to keep the forebody vortex on this side close to the surface and increase its strength. The effect is not obtainable on a diamond forebody due to the sharp top edge that promotes secondary separation along its length. This separation leads to the formation of a strong secondary vortex with an opposite sense of rotation as its corresponding primary vortex.

Acknowledgment

Financial support for this research was provided by the Ohio Board of Regents under the Research Challenge program.

References

[1]Hall, R. M., Erickson, G. E., Straka, W. A., Peters, S. E., Maines, B. H., Fox, M. C., Hames, J. E., and LeMay, S. P., "Impact of Nose-Probe Chines on the Vortex Flows About the F-16C," AIAA Paper 90-0386, 1990.

[2]Stahl, W., "Suppression of Asymmetry of the Vortex Flow Behind a Circular Cone at High Incidence," AIAA Paper 89-3372, Aug. 1989.

[3]Ng, T. T., "The Effect of a Single Strake on the Forebody Vortex Asymmetry," *Journal of Aircraft*, Vol. 27, No. 9, 1990, pp. 844–846.

[4]Murri, D. G., and Rao, D. M., "Exploratory Studies of Actuated Forebody Strakes for Yaw Control at High Angles of Attack," AIAA Paper 87-2557, Aug. 1987.

[5]Malcolm, G. N., Ng, T. T., Lewis, L. C., and Murri, D. G., "Development of Non-Conventional Control Methods for High Angle of Attack Flight Using Vortex Manipulation," AIAA Paper 89-2192, Jan. 1989.

[6]Moskovitz, C., Hall, R., and DeJarnette, F., "Experimental Investigation of a New Device to Control the Asymmetric Flowfield on Forebodies at Large Angles of Attack," AIAA Paper 90-0068, Jan. 1990.

[7]Ng, T. T., and Malcolm, G. N., "Aerodynamic Control Using Forebody Strakes," AIAA Paper 91-0618, Jan. 1991.

[8]Tavella, D. A., Schiff, L. B., and Cummings, R. M., "Pneumatic Vortical Flow Control at High Angles of Attack," AIAA Paper 90-0098, Jan. 1990.

[9]Ng, T. T., and Malcolm, G. N., "Aerodynamic Control Using Forebody Blowing and Suction," AIAA Paper 91-0619, Jan. 1991.

[10]Erickson, G. E., and Brandon, J. M., "Low-Speed Experimental Study of the Vortex Flow Effects of a Fighter Forebody Having Unconventional Cross-Section," AIAA Paper 85-1798, Jan. 1985.

[11]Brandon, J. M., and Nguyen, L. T., "Experimental Study of Effects of Forebody Geometry on High Angle of Attack Static and Dynamic Stability," AIAA Paper 86-0331, Jan. 1986.

[12]Erickson, G. E., and Brandon, J. M., "On the Nonlinear Aerodynamic and Stability Characteristics of a Generic Chine-Forebody Slender-Wing Fighter Configuration," AIAA Paper 87-2617, Jan. 1987.

[13]Roos, F. W., and Kegelman, J. T., "Aerodynamic Characteristics of Three Generic Forebodies at High Angles of Attack," AIAA Paper 91-0275, Jan. 1991.

[14]Guyton, R. W., Osborn, R. F., and LeMay, S. P., "Forebody Vortex Control Aeromechanics," AGARD FDP Specialisits' Meeting on Manoeuvring Aerodynamics, Toulouse, France, May 1–2, 1991.

[15]Iwanski, K. P., "Advances Fighter Mechanical Forebody Vortex Flow Control," Aeromechanics Div., Wright Lab., TR WL-TM-91-310, Dayton, OH, 1991.

[16]Rao, D., and Sharma, G., "Mechanical and Pneumatic Side-Force Control Investigations of a Diamond Cross-Section Forebody at High Angles of Attack," AIAA Paper 93-3407, Aug. 1993.